optics

MDPI

Article

Design of a Highly Sensitive Detector Using a Ternary Photonic Crystal (PC) Based on Titanium Nitride Sandwiched between Si and SiO_2 for the Creatinine Concentration Detection in the Blood Serum

Malek G. Daher [1,*], Youssef Trabelsi [2,3], Abinash Panda [4], Ashot H. Gevorgyan [5], Khedr M. Abohassan [6], Lassaad K. Smirani [7,8], Baraa Riyadh Altahan [9] and Ahmed Nabih Zaki Rashed [10]

1 Physics Department, Islamic University of Gaza, Gaza P.O. Box 108, Palestine
2 Physics Department, College of Arts and Sciences in Muhail Asir, King Khalid University, Abha 62529, Saudi Arabia
3 Photovoltaic and Semiconductor Materials Laboratory, National Engineering School of Tunis, University of Tunis El Manar, Tunis 1002, Tunisia
4 Department of Electronics and Communication Engineering, National Institute of Technology Silchar, Silchar 788010, India
5 School of Natural Sciences, Far Eastern Federal University, 10 Ajax Bay, Russky Island, 690922 Vladivostok, Russia
6 Department of Mathematics and Sciences, Dhofar University, Salalah 211, Oman
7 Elearning Deanship and Distance Education, Umm Al-Qura University, Mecca 24381, Saudi Arabia
8 InnoV'COM Lab, University of Carthage, Ariana 2027,Tunisia
9 Medical Instrumentation Techniques Engineering Department, Al-Mustaqbal University College, Hilla 51001, Iraq
10 Electronics and Electrical Communications Engineering Department, Faculty of Electronic Engineering, Menoufia University, Menouf 32951, Egypt
* Correspondence: malekjbreel20132017@gmail.com

check for updates

Citation: Daher, M.G.; Trabelsi, Y.; Panda, A.; Gevorgyan, A.H.; Abohassan, K.M.; Smirani, L.K.; Altahan, B.R.; Rashed, A.N.Z. Design of a Highly Sensitive Detector Using a Ternary Photonic Crystal (PC) Based on Titanium Nitride Sandwiched between Si and SiO_2 for the Creatinine Concentration Detection in the Blood Serum. *Optics* **2022**, *3*, 447–461. https://doi.org/10.3390/opt3040038

Academic Editors: Thomas Seeger, Amit kumar Goyal and Yuri Kivshar

Received: 22 September 2022
Accepted: 25 November 2022
Published: 29 November 2022

Abstract: It is very important to design a rapid and sensitive device for the creatinine concentration detection due to it being one of the most considerable benchmarks for efficient kidney working. Here, a novel biophotonic sensor using one-dimensional ternary PC based on $Si/TiN/SiO_2$ layers is proposed for the creatinine concentration detection in a blood serum sample. A central cavity layer is inserted between two equal periodic numbers. The blood sample can be infiltrated in the cavity layer with various creatinine concentrations. Based on the technique of transfer matrix, the transmittance spectra properties are investigated. The influences of variation of the incidence angle for both TE and TM polarizations and the cavity layer thickness are carefully investigated to attain the best sensitivity of the biophotonic detector. A high sensitivity of 938.02 nm/RIU is realized for the suggested detector, which is comparable to most recent works published in this area. Moreover, the proposed sensor has an inexpensive cost, real-time detection, and simple structure, which is helpful to the industrial design using low-cost product nanofabrication techniques. Based on above-mentioned outcomes, our biosensor candidate is a suitable and effective device for the detection of creatinine concentration, and it can use for any biological sample.

Keywords: ternary photonic crystal; creatinine concentration; titanium nitride; transfer matrix; sensitivity

1. Introduction

Recently, the research in nano-optoelectronic devices gathered a large amount attention by physicists and engineers for their various and enormous applications [1]. Multiple layers with high and low refractive indices make up a photonic crystal (PC), which governs the travel of light [2]. One-dimensional (1D), two-dimensional (2D), and three-dimensional (3D) PC can be categorized based on the repeated dimensions [3]. In addition, PC structures

can be sorted into binary (two layers in one period), ternary (three layers in one period), and quaternary (four layers in one period) based on the number of layers in each cell (period). The presence of a photonic band gap (PBG) in the transmittance profile of PCs is a crucial characteristic [4]. Consequently, PCs have been considerably utilized in a variety of applications, including as a narrowband filter [5], an optical absorber [6], and an optical mirror [7], as well as for optical sensing [8], a polarization manipulating device [9], and optical binding [10]. Given that the scaling factor of the PC fabrication process from micro- to nanoscales was well-matched for both the IR and visible areas [11], photonic crystals (PCs) have been used as a temperature sensor [12], biosensor [13], chemical sensor [14], hydrostatic pressure detector [15], and gas sensor [16].

Creatinine is a chemical waste excreted with metabolic processes in biological systems. It is very important for the energy production in muscles. The process of creatinine clearance from the biological system is essential. This action occurs by the body disposing of creatinine in urine after it transfers through the blood to the kidney. Thus, the creatinine levels in blood are measured as important benchmarks for kidney performance [17,18]. Thus, the sensing process of creatinine concentration in the blood is an essential stage to detect kidney diseases [19,20]. There are several techniques to decide levels of creatinine in blood, such as Jaffe's method [21], as well as enzymatic methods [22,23].

Here, a one-dimensional ternary photonic crystal (1D-TPC) with a defective layer utilized as a biophotonic sensor for the creatinine concentration detection in blood serum. A ternary PC was chosen because it is more sensitive compared to binary PCs. The transfer matrix approach was employed to investigate the spectra of transmittance of the suggested structure. The influences of incident angle (TE and TM polarizations) and defect layer thickness were checked. The proposed detector's greatest sensitivity was computed and contrasted with the most recent sensors, which is related to biosensing.

2. Theoretical Method

According to Figure 1, a ternary photonic crystal (TPC) with the $(A_1A_2A_3)N/D/(A_1A_2A_3)N$ structure is assumed. The layers A_1, A_2, and A_3, are Si, TiN, and SiO_2, respectively. D is the cavity that sits in the middle of two similar periodic structures. Air surrounds the TPC on both sides. N is the number of periods.

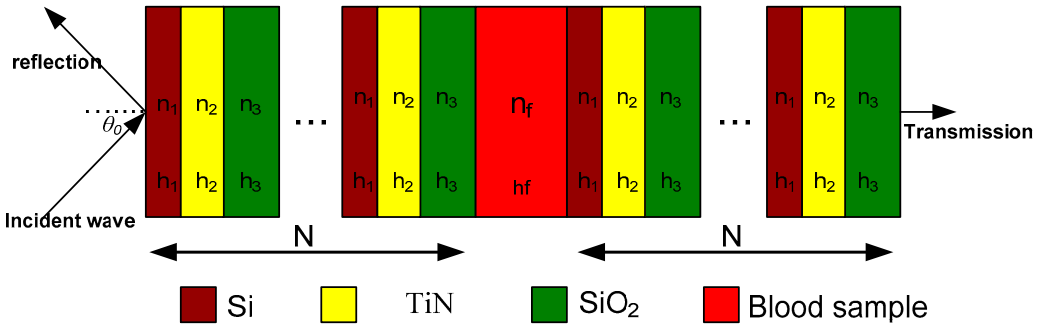

Figure 1. Graphical depiction of a 1D-TPC with a defect layer.

The optical properties of PCs can be simulated and investigated using several techniques. For a 1D PCs, the optical properties can be studied using a lot of the mathematical techniques such as the transfer matrix and finite element methods. As a straightforward and adaptable method for examining the optical characteristics of 1D periodic structures, such as transmission and reflection spectra, we shall employ the transfer matrix approach. One layer's (E_j) characteristic matrix can be expressed as

$$E_j = \begin{bmatrix} \cos(Y_j) & -\frac{i \sin(Y_j)}{\varphi_j} \\ -i\varphi_j \sin(Y_j) & \cos(Y_j) \end{bmatrix} \quad (1)$$

Y_j is the jth layer's phase variation, where

$$Y_j = \frac{2\pi}{\lambda} n_j h_j \cos\theta_j \tag{2}$$

where n_j is the refractive index and h_j is the thickness. θ_j is the incident angle into the layer which is expressed with the initial incidence angle θ_0 as

$$\cos\theta_j = \sqrt{1 - \left(\frac{n_0 \sin(\theta_0)}{n_j}\right)^2} \tag{3}$$

$\varphi_j = n_j \cos(\theta_j)$ for the transverse electric (TE) wave, $\varphi_j = \cos(\theta_j)/n_j$ for the transverse magnetic (TM) wave, and n_0 is the refractive index of the incidence medium. The matrix E_0 for one cell comprising three layers A_1, A_2, and A_3 can be printed as $E_0 = E_{A1}$ E_{A2} E_{A3}. The full transfer matrix X of a defective TPC can be written as

$$X = (E_0)^N E_D (E_0)^N = \begin{bmatrix} X_{11} & X_{12} \\ X_{21} & X_{22} \end{bmatrix} \tag{4}$$

The elements of the complete transfer matrix X are Xij, and E_D is the transfer matrix of the cavity medium. The coefficient of transmission (t) can be expressed as

$$t = \frac{2\varphi_{in}}{(X_{11} + X_{12}\varphi_{out})\varphi_{in} + (X_{21} + X_{22}\,\varphi_{out})} \tag{5}$$

and the transmittance can write as the form

$$T = \frac{\varphi_{out}}{\varphi_{in}} |t|^2 \tag{6}$$

The TPC is intended to be surrounded by air. Thus, $\varphi_{in} = \varphi_{out} = \cos(\theta_0)$ for both (TE) and (TM) polarizations.

3. Results and Discussion

3.1. Creatinine Concentration Biosensor

A photonic crystal having the structure $(Si/TiN/SiO_2)^N$/defect $(Si/TiN/SiO2)^N$ is applied as a creatinine sensor. The refractive indices of the layers are 3.3 (for Si), 1.28 (for TiN), and 1.46 (for SiO_2). It is worth mentioning that TiN demonstrates some crucial assets such as amazing thermal stability, soft optical loss, and chemical inertness. Owing to its high thermal stability and high field improvements, a TiN-based photonic structure can be the appropriate candidate for optical sensing devices with high performance [24]. In general, ternary PC is chosen because it is more sensitive compared to binary PCs [25]. Therefore, we can use another layer other than titanium dioxide with similar properties to install a ternary photonic crystal. The thicknesses are selected as h_1 = 120 nm, h_2 = 260 nm, and h_3 = 190 nm. The assumed number of periods is N = 4. D is the cavity layer to be treated as a blood sample with different concentrations of creatinine. In Table 1, the refractive indices for various concentrations in µmol/L of creatinine in a blood sample is given [26,27] and is shown in Figure 2 (red points). Using a mathematic program, the index-concentration relation's polynomial fit is provided by

$$RI(C) = -849.40 + 30.75\,C - 0.369725\,C^2 + 0.00148011\,C^3 \tag{7}$$

where $RI(C)$ is the refractive index and C is the creatinine concentration. Any C-value can be predicted using Equation (7) for a blood sample's refractive index. The fitted index as a function of the creatinine concentration is illustrated is Figure 2 (black curve). Normal incidence ($\theta_0 = 0^\circ$) is first studied, which is the same for both TE and TM modes, and

the thickness of defective cavity is selected as h_f = 500 nm. The transmittance spectrum through the suggested TPC without any defective layer is exhibited in Figure 3a. A wide PBG of width of 1243.19 nm can be observed with left and right ends at wavelengths of 1580 nm and 2823.19 nm, respectively. Figure 3b displays the transmittance spectrum of the proposed structure when the defect layer is filled with a blood sample at a concentration of creatinine of 80.9 µmol/L and 82.3 µmol/L. The width of the PBG grows to 1243.88 nm where the right and left ends are at wavelengths of 2783.69 nm and 1539.81 nm, respectively. It is noted that the width of PBG did not change, but a little shift occurred in the direction of the left side. With an enlarged view inside Figure 3, two defect modes can be noticed at a resonant wavelength of 1871.76 nm and 1864.47 nm for C = 80.9 and 82.3 µmol/L, respectively. It is observed that the defect peak shifted toward the lower wavelength when a blood sample (C = 82.3 µmol/L) instead of the blood sample (80.9 µmol/L). This swing of defect peak is due to the defect mode's location-dependent refractive index, which complies with the standing wave requirement [28]:

$$OPD = n_{eff}\, L = J\, \lambda \tag{8}$$

where OPD, J, n_{eff}, and L are the difference of optical path, effective index of refractive, difference of geometric path and an integer number, respectively. The sensitivity of these modes is calculated and found to be 331.36 nm/RIU (refractive index unit). In the next sections, we optimize both the incident angle for TE and TM polarization and thickness of cavity layer to obtain a higher sensitivity of the proposed TPC sensor.

Table 1. The blood sample's refractive index at various concentrations of creatinine.

Creatinine Concentration (µmol/L)	80.9	81.43	82.3	83.3	84.07	85.28
Refractive index	2.661	2.655	2.639	2.610	2.589	2.565

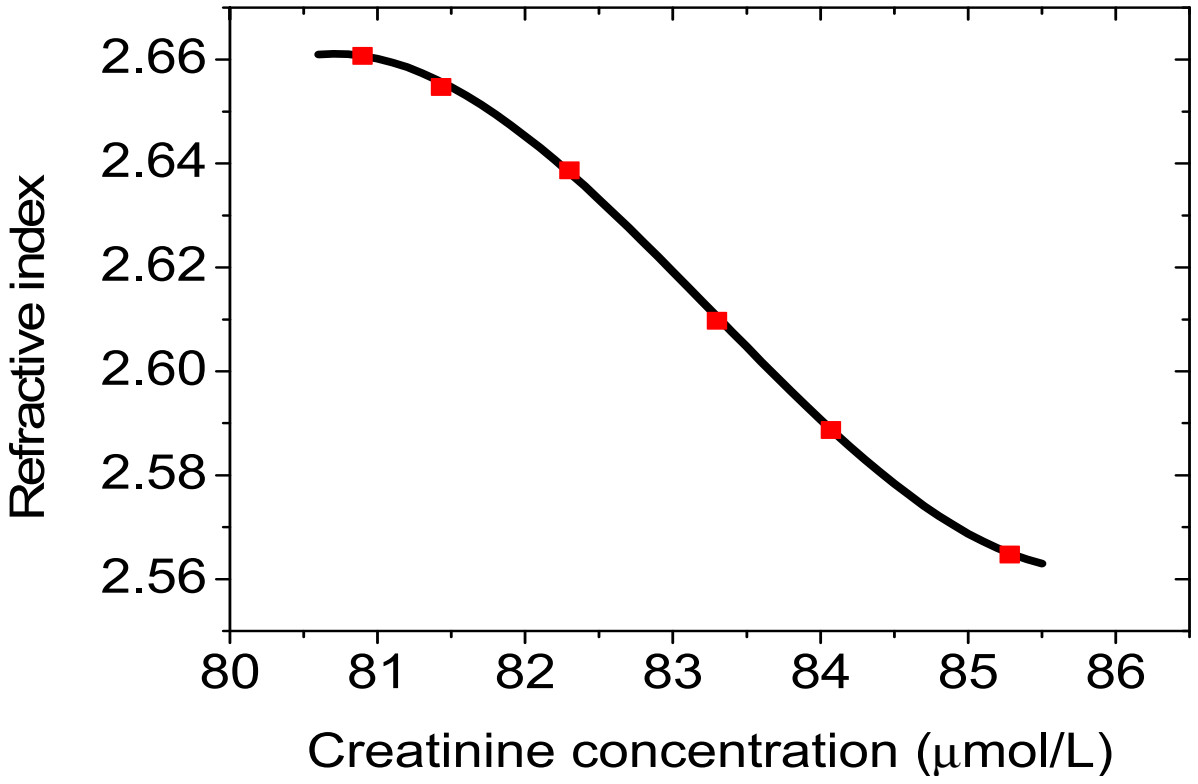

Figure 2. Index of refraction of the blood sample versus the creatinine concentration in µmol/L.

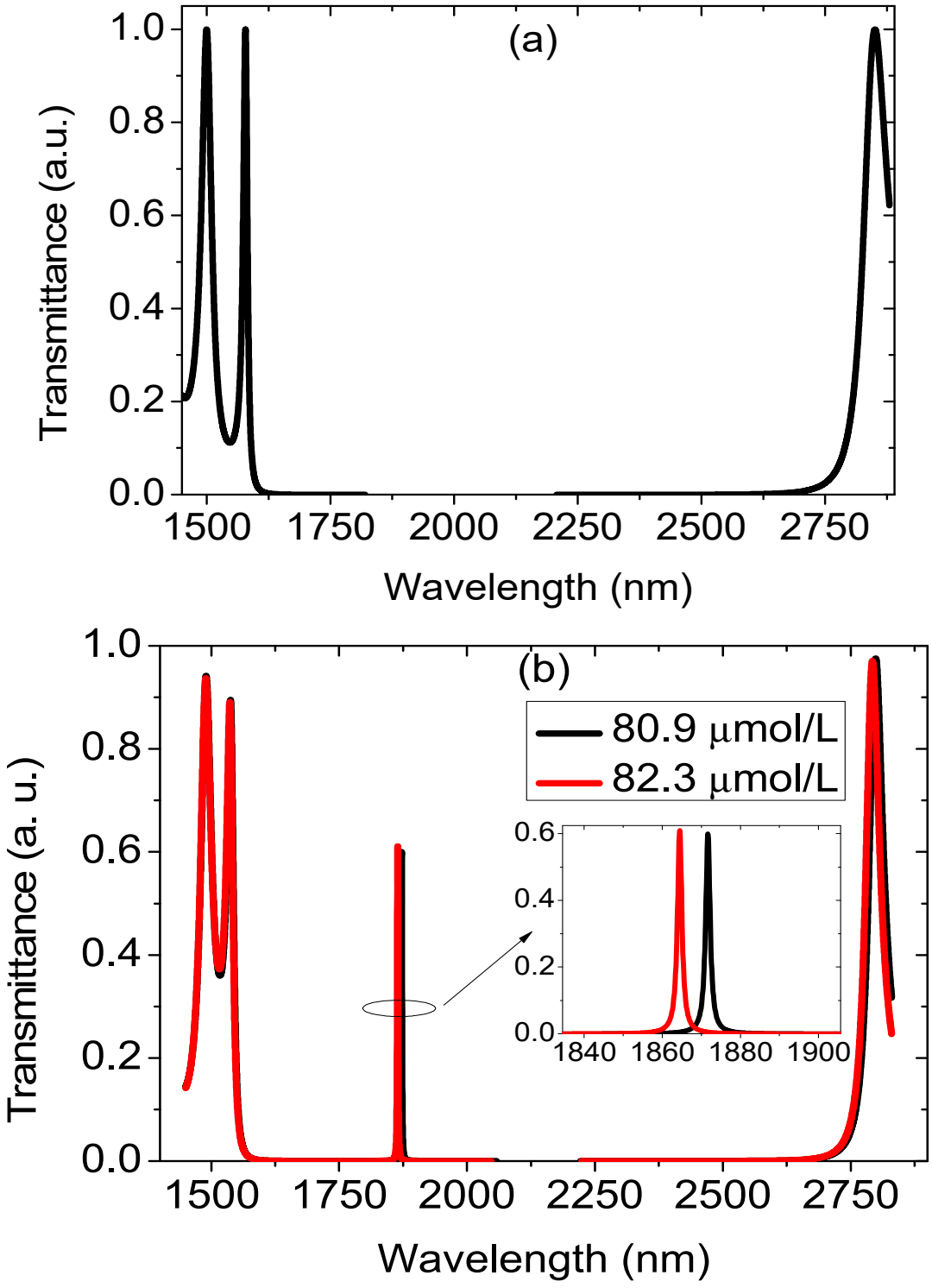

Figure 3. Transmittance spectra of TPC (**a**) without a defect medium; (**b**) with a defect medium at $\theta_0 = 0.0°$, $h_1 = 120$ nm, $h_2 = 260$ nm, $h_3 = 190$ nm, $h_3 = 500$ nm, $n_1 = 3.3$, $n_2 = 1.28$, $n_3 = 1.46$.

3.2. Effect of Variation in the Incident Angle

In this section, the transmittance spectra was investigated for both TE and TM waves when the cavity layer thickness was fixed as $h_f = 500$ nm and the angle of incidence was adjusted in 10-degree steps from 0° to 70°. The spectrum of transmission is exhibited in Figure 4a–d (TE polarization) and Figure 5a–d (TM polarization) corresponding to incident angles 0°, 20°, 40°, and 60°, respectively. The transmission spectra of Figures 4 and 5 show

the reaction as the cavity region in the proposed structure was infiltrated separately with blood samples for two concentrations of creatinine (80.9 µmol/L and 82.3 µmol/L). With an increase in creatinine concentration, the defect mode shifts toward a lower wavelength. Because blood samples' refractive indices drop as their creatinine concentrations rise, the defect peaks within the transmittance spectra shift in response. Moreover, the increase in the incidence angle at the same concentration of creatinine causes movement of the defect peaks toward the lower wavelength region with reduction in their intensity, as observed in Figure 4a–d (TE polarization), and with growth in their intensity, as seen in Figure 5a–d (TM polarization). The blue shift of the defect mode with an increasing of incident angle can be explained based on Bragg Snell's law [29]:

$$s\,\lambda = 2\,g\left(n_{eff}^2 - \sin^2\theta_0\right)^{0.5} \tag{9}$$

where s, λ, g, n_{eff}, and θ_0 are the diffraction order (s = 1, 2, 3, . . .), the free space wavelength, the interplanar spacing, the effective index of refractive, and the angle of incidence, respectively.

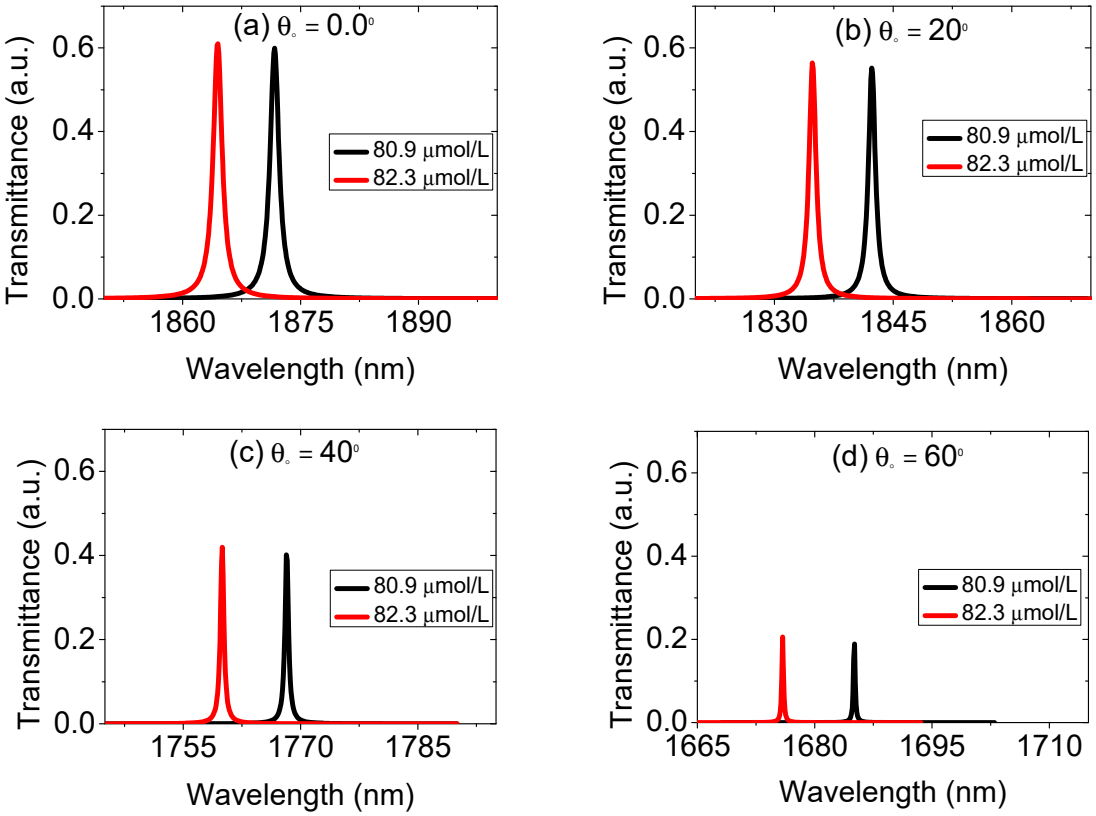

Figure 4. Transmittance curves of the suggested TPC biosensor with different incident angles (**a**) 0.0°, (**b**) 20°, (**c**) 40°, and (**d**) 60° for the TE mode.

It is also noted that the increase in the incident angle shrinks the intensity of each defect peak faintly without influencing the detecting capabilities and qualifications of the biosensor. Figure 6 shows the sensitivity improvement for TE polarization is higher than TM polarization as the incident angle increases, which is a very important condition in the design of optical sensing devices. The sensitivity was calculated and found to rise from 331.36 to 429.09 nm/RIU when the incident angle increased from θ_0 = 0.0° to θ_0 = 70° for the TE case. We also observed a little enhancement of the sensitivity with an increase in the incident angle for the TM case. The sensitivity increased from 331.36 (θ_0 = 0.0°) to 340 nm/RIU (θ_0 = 40°), and after that, the sensitivity started declining. Figure 6 exhibits the behavior of the sensitivity with the angle of incidence. The calculations of the defect mode

positions, wavelength shift, and sensitivity for all these angles are presented for TE (Table 2) and TM (Table 3) polarizations. At $\theta_0 = 60^\circ$, the movement of the defect peaks through the PBG is toward the lower wavelength side with progressed sensitivity and acceptable intensity of defect modes. It is observed that the defect modes of TE polarization are sharper than those of TM polarization, which is one of the fundamental requirements for any good-quality optical sensor. When we compare the findings of TE and TM polarizations, we find the case of TE is better than that of TM polarization. It is worth noting that for angles larger than $\theta_0 = 60^\circ$ in the TE case, the defect modes are very small, which is undesirable in the design of sensing devices. Thus, the incident angle of $\theta_0 = 60^\circ$ for TE polarization is the optimum value because it has improved sensitivity, sharp peaks, and acceptable intensity of defect modes that are sufficiently and easily sensed by the transducer of the reported biophotonic detector design.

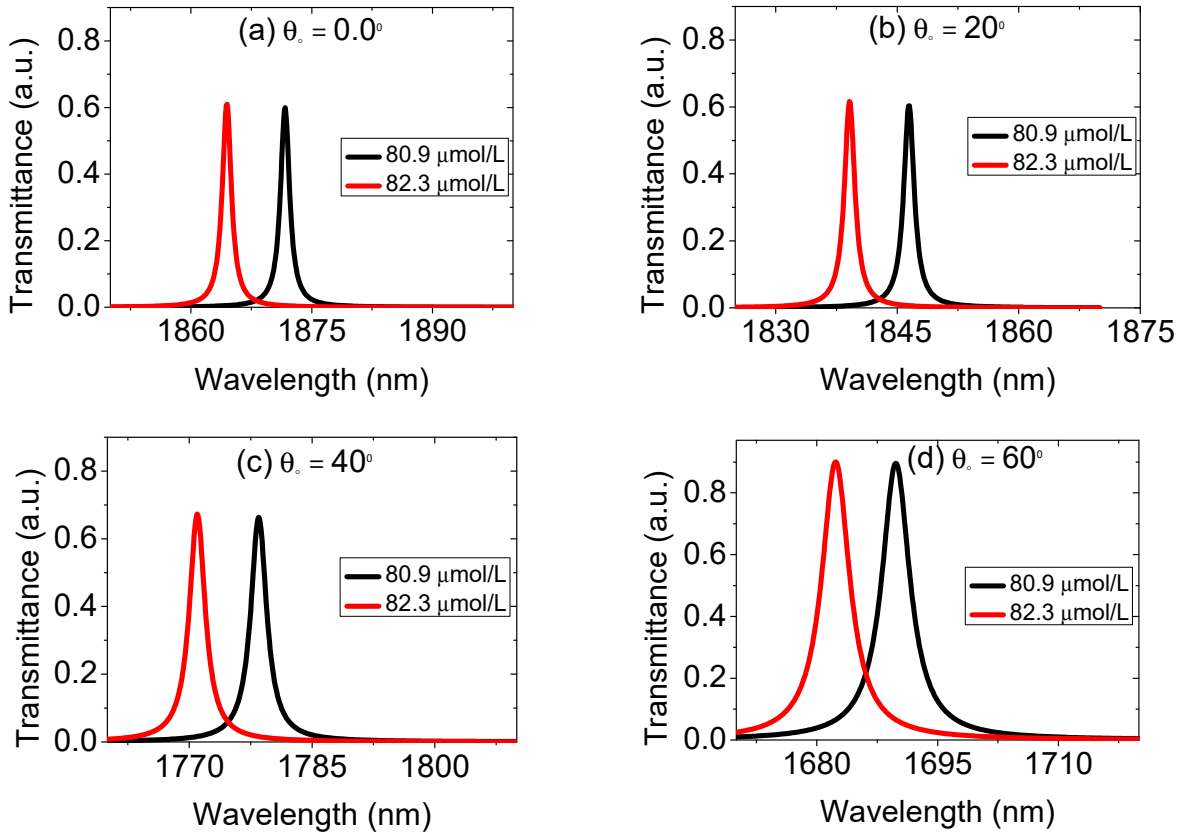

Figure 5. Transmittance curves of the suggested TPC biosensor with different incident angles (**a**) 0.0°, (**b**) 20°, (**c**) 40°, and (**d**) 60° for the TM mode.

Table 2. Position of resonant peak and sensitivity (S) of creatinine concentration for different incident angles at $n_1 = 3.3$, $n_2 = 1.28$, $n_3 = 1.46$, $h_1 = 120$ nm, $h_2 = 190$ nm, $h_3 = 260$ nm, $h_f = 500$ nm, and $N = 4$ (TE mode).

Incident Angle (θ_0)	Position of Resonant Peak at C = 80.9 (mmol/L)	Position of Resonant Peak at C = 82.3 (mmol/L)	Shift of Wavelength (nm)	S (nm/RIU)
0.0	1871.76	1864.47	7.29	331.36
10	1864.17	1856.85	7.32	332.72
20	1842.34	1834.89	7.45	338.63
30	1809	1801.17	7.83	355.90
40	1768.3	1760.02	8.28	376.36
50	1725.21	1716.52	8.69	395
60	1685.11	1675.96	9.15	415.90
70	1652.73	1643.29	9.44	429.09

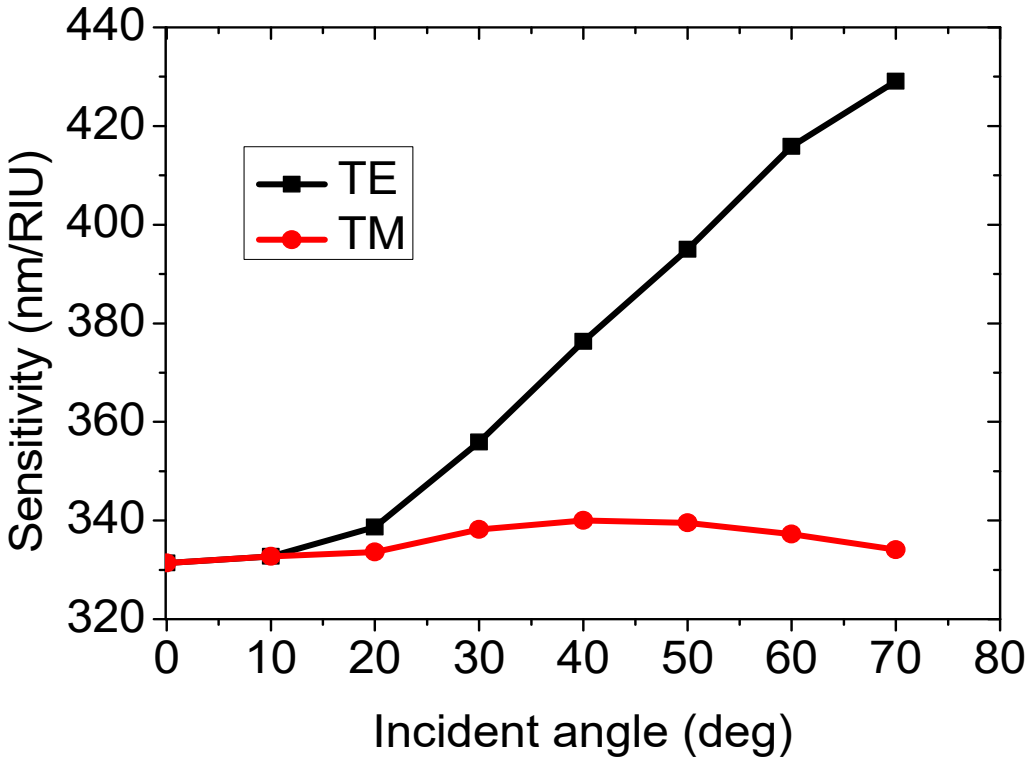

Figure 6. Sensitivity versus incident angle for both TE and TM modes at h_f = 500 nm.

Table 3. Position of resonant peak and sensitivity (S) of creatinine concentration for different incident angles at n_1 = 3.3, n_2 = 1.28, n_3 = 1.46, h_1 = 120 nm, h_2 = 190 nm, h_3 = 260 nm, h_f = 500 nm, and N = 4 (TM mode).

Incident Angle (θ_0)	Position of Resonant Peak at C = 80.9 (μmol/L)	Position of Resonant Peak at C = 82.3 (μmol/L)	Shift of Wavelength (nm)	S (nm/RIU)
0.0	1871.76	1864.47	7.29	331.36
10	1865.33	1858.01	7.32	332.72
20	1846.5	1839.16	7.34	333.63
30	1816.8	1809.36	7.44	338.18
40	1778.51	1771.03	7.48	340
50	1734.82	1727.35	7.47	339.54
60	1689.83	1682.41	7.42	337.27
70	1649.07	1641.72	7.35	334.09

3.3. Effect of Variation in the Thickness of Defective Cavity

In this section, we inspect how the thickness of defective cavity influences the sensitivity of the suggested TPC biosensor under conditions of normal incidence. For this target, we scanned the thickness of the cavity layer from 0.5 μm to 5.5 μm with a step of 0.5 μm. The transmittance spectra of the suggested photonic structure corresponding to a cavity layer of thicknesses 1.5, 2.5, 3.5, and 4.5 μm are shown in Figure 7a–d, respectively. Transmittance spectra of Figure 7 exhibit that, due to an increase in the thickness of the cavity layer under conditions of normal incidence corresponding to blood samples whose refractive indices change from higher to lower value, the defect modes inside the photonic BG shift their location toward a lower wavelength. Figure 6 shows the sensitivity development when the cavity's thickness increases, which is, again, one of the central qualifications for any good biophotonic sensor. It can be seen that the sensitivity climbs from 331.36 to 841.36 nm/RIU

as the thickness of the cavity layer rises from h_f = 0.5 µm to h_f = 5.5 µm, as shown in Figure 8. By increasing the thickness of the cavity layer to greater than h_f = 5.5 µm, a few increases in the sensitivity are noticed. As a result, the optimal thickness of the cavity layer is h_f = 5.5 µm. Moreover, their intensity gradually grows and reaches the maximum at a cavity layer of thickness 5.5 µm. The maximum value of intensity is always desired for a good-performing biophotonic sensor. As the thickness of the cavity layer increases, the electromagnetic wave will have a longer geometric path through the cavity, and a greater interaction occurs between the incident wave and the sensing sample. As a result, the sensitivity and intensity of peaks are improved. Thus, the optimum thickness of the cavity layer is selected as 5.5 µm. The calculations of defect mode positions, wavelength shift, and sensitivity for all these thicknesses of cavity layers are presented in Table 4.

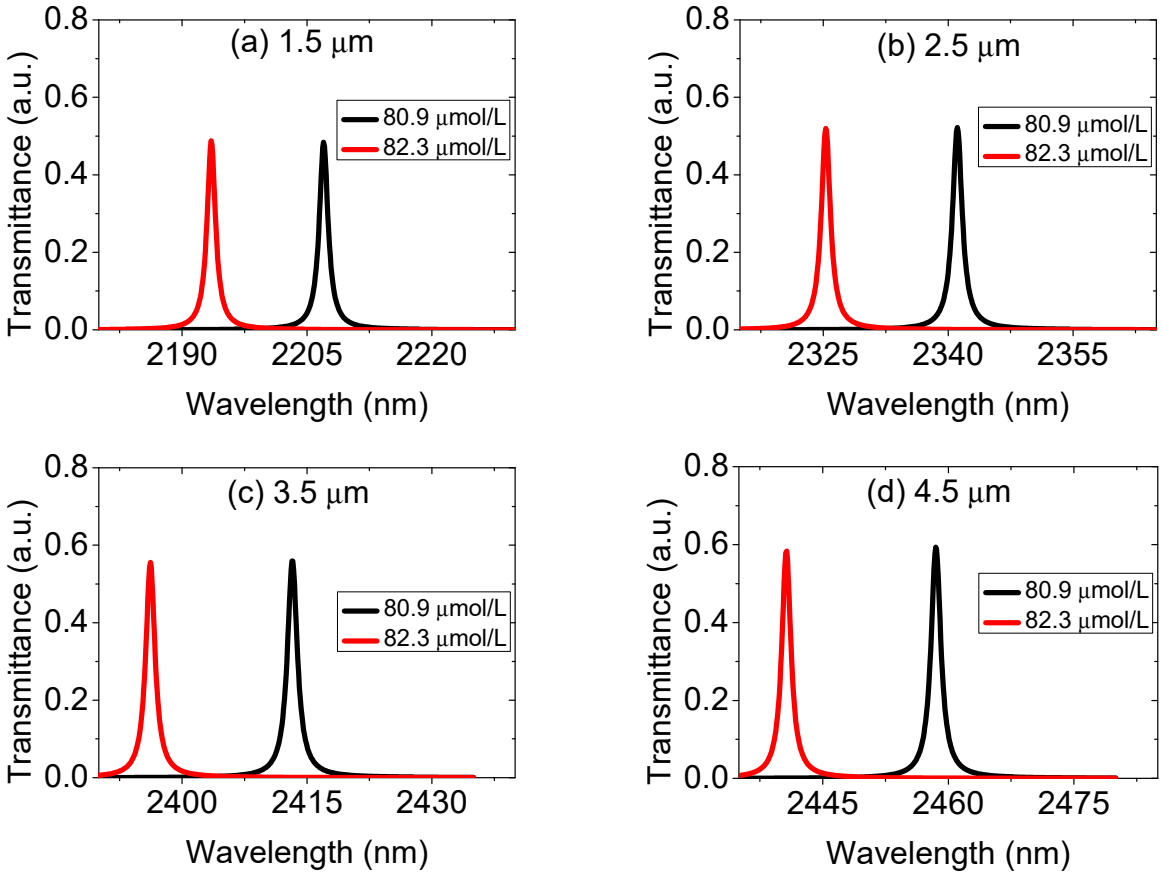

Figure 7. Transmittance curves of the suggested TPC biosensor with different thicknesses of cavity layers: (**a**) 1.55 µm, (**b**) 2.55 µm, (**c**) 3.55 µm, and (**d**) 4.5 µm at $\theta_0 = 0°$.

3.4. Analysis of the Optimum Case for the Proposed Structure

Based on the aforementioned outcomes, we found the optimized case at which the proposed biophotonic sensor works efficiently occurs at a thickness of cavity layer h_f = 5.5 µm and an incident angle $\theta_0 = 60°$. At this optimum state, Figure 9 shows the spectrum of transmittance for different concentrations of creatinine (80.9, 81.43, 82.3, 83.3, 84.07, and 85.28 µmol/L). It is worth to note that we fixed other structural parameters in this work in order to achieve a broader photonic BG, which gave us the ability to examine a larger number of blood samples for different concentrations of creatinine. It can be seen that the defect peaks inside the photonic BG change their place toward lower wavelengths as the concentration of creatinine grows. This shifting of the defect peak through the photonic BG is due to the decrease in the blood sample index as the concentration of creatinine rises.

The polynomial relation between the resonant wavelength of defect mode (*RW*) and the concentration of creatinine (*C*) of the proposed TPC biosensor can be fitted and written as

$$RW(C) = -790602 + 28623.8\ C - 344.02\ C^2 + 1.37\ C^3 \quad (10)$$

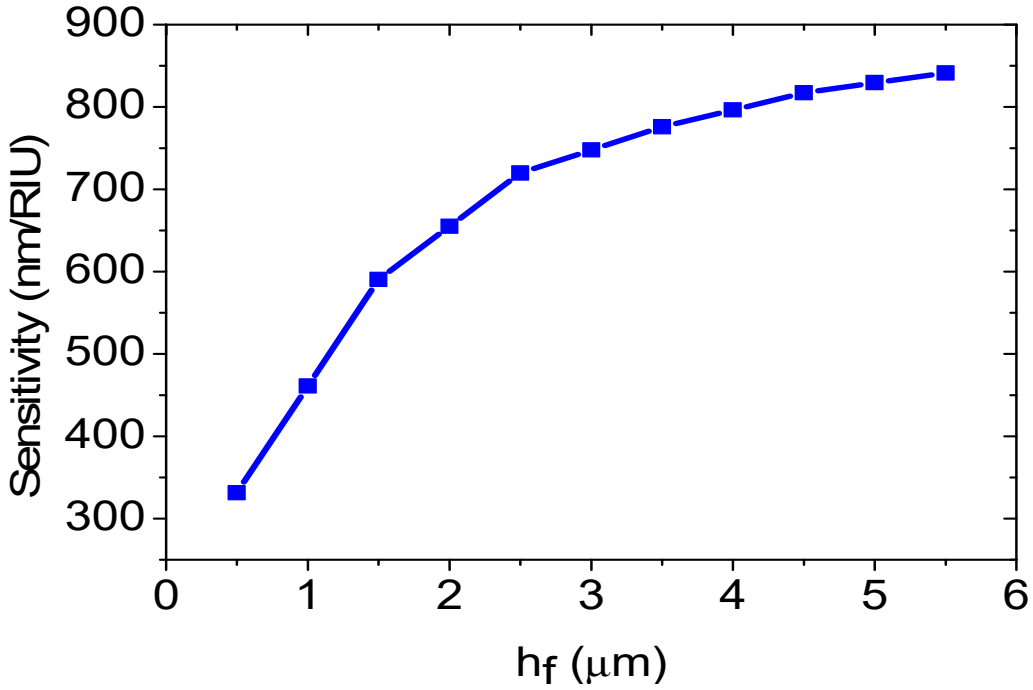

Figure 8. Sensitivity versus thickness of defect layer at $\theta_0 = 0°$ and $N = 4$.

Table 4. Position of resonant peak and sensitivity of creatinine concentration for different thicknesses of defect layer at $\theta_0 = 0.0°$ and $N = 4$.

Thickness of Cavity Layer (μm)	Position of Resonant Peak at *C* = 80.9 (μmol/L)	Position of Resonant Peak at *C* = 82.3 (μmol/L))	Shift of Wavelength (nm)	*S* (nm/RIU)
0.5	1871.76	1864.47	7.29	331.36
1	2039.38	2029.24	10.14	460.90
1.5	2207	2194.01	12.99	590.45
2	2274.09	2259.68	14.41	655
2.5	2341.19	2325.36	15.83	719.54
3	2377.24	2360.79	16.45	747.72
3.5	2413.3	2396.23	17.07	775.90
4	2435.93	2418.41	17.52	796.36
4.5	2458.57	2440.59	17.98	817.27
5	2474.14	2455.89	18.25	829.54
5.5	2489.71	2471.2	18.51	841.36

Equation (8) can be employed to predict the resonant position of the peak for any concentration of creatinine. Table 5 shows the numerically calculated positions of the resonant peak, shift of wavelength, and sensitivity of creatinine biosensor. This table presents the sensitivity variation of the suggested structure between 928.33 nm/RIU and 938.02 nm/RIU under the effect of various concentrations of creatinine. Moreover, the polynomial relation

between the sensitivity (S) of our biophotonic sensor and the concentration of creatinine in the blood (C) of the suggested TPC biosensor can be fitted and expressed as

$$S(C) = 17186.7 - 570.31\ C + 6.634\ C^2 - 0.025576\ C^3 \quad (11)$$

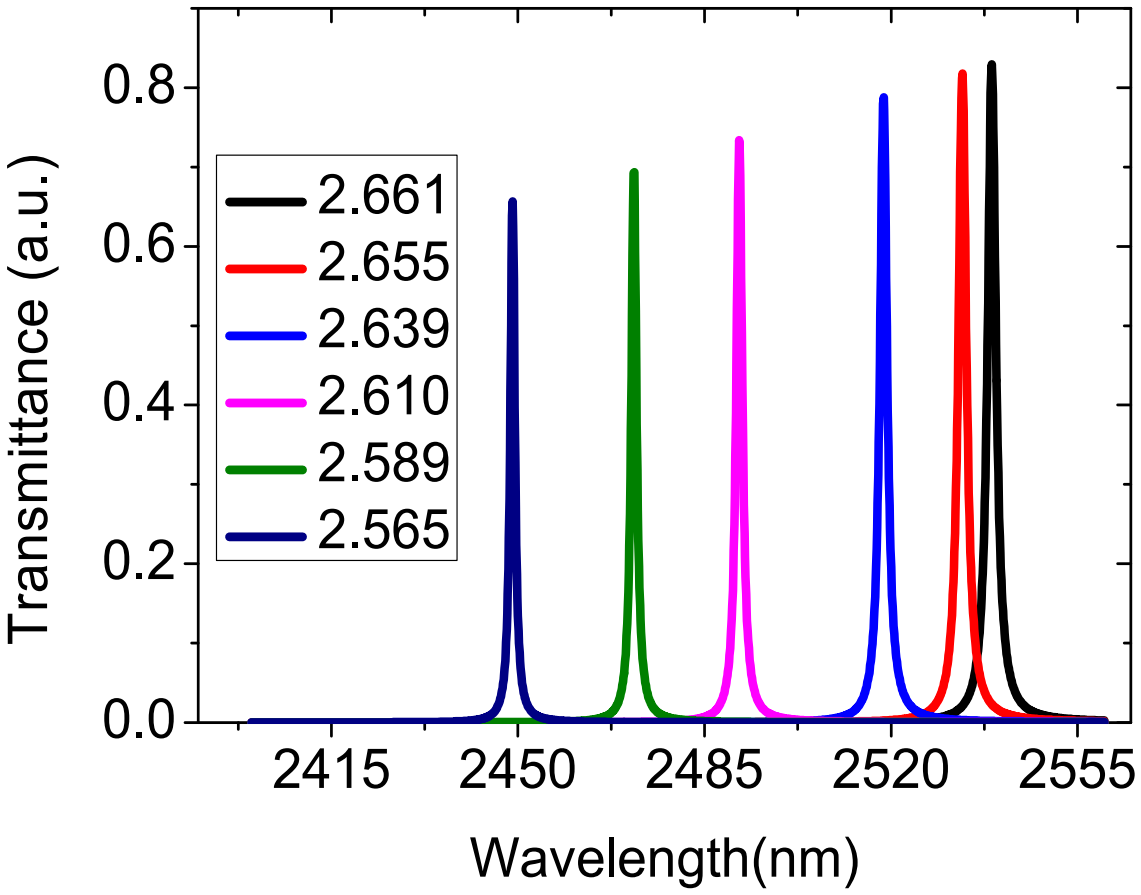

Figure 9. Transmittance spectra of the suggested TPC biosensor for various concentrations of protein at $\theta_0 = 60°$, $h_f = 5.5$ µm, and $N = 4$.

Table 5. Position of resonant peak and sensitivity of different concentrations of creatinine in blood serum at $h_1 = 120$ nm, $h_2 = 190$ nm, $h_3 = 260$ nm, $\theta_0 = 60°$, $h_f = 5.5$ µm, and $N = 4$.

Creatinine Concentration (µmol/L)	Index of Refraction	Resonant Peak Position (nm)	Shift of Wavelength (nm)	*S* (nm/RIU)
80.9	2.661	2539	-	-
81.43	2.655	2533.43	5.57	928.33
82.3	2.639	2518.58	20.42	930
83.3	2.610	2491.47	47.53	931.96
84.07	2.589	2471.72	67.28	934.44
85.28	2.565	2448.95	90.05	938.02

It is clear that the equivalents between the fitting curves and simulated data are quite a good match, as is shown in Figures 10 and 11 for resonant wavelength and sensitivity, respectively. Here, it is noteworthy that the sensitivity of the proposed biophotonic sensor is ultra-high and can be used for other biosensing. The suggested biosensor designed (by alternating $Si/TiN/SiO_2$) with a creatinine sample as a defect layer demonstrated an efficient sensitivity reach to 938.02 nm/RIU, which is not realized for a lot of recently

published articles related to biosensing. For example, in 2020, Arafa H Aly et. al. searched the sensitivity of a 1D photonic crystal with a cavity layer for creatinine concentration detection in blood, and they achieved a sensitivity of 306 nm/RIU. As another example, the maximum sensitivity was reported to be 640.29 nm/RIU in 2021 by Sakshi Gandhi, who examined the sensitivity of a biosensor for the creatinine detection in levels of blood serum. Here, in comparison to all of these recent publications, the proposed biophotonic sensor that is presented in this work demonstrated the highest sensitivity. Table 6 compares the sensitivity of the suggested biosensor to the most contemporary biosensing designs. Giving some advice about how to fabricate the proposed sensor is really important. Using the nanoimprint lithography technology, the proposed structure can be generated easily. The photonic crystal can be incorporated into a waveguide to describe the built system. A cavity is introduced between two identical numbers of periods and can be treated as a sensing medium. The cavity is filled with the sensing sample, and the structure is illuminated by a light source. To exhibit and inspect the transmitted beam, an optical detector is necessary on the other side of the system.

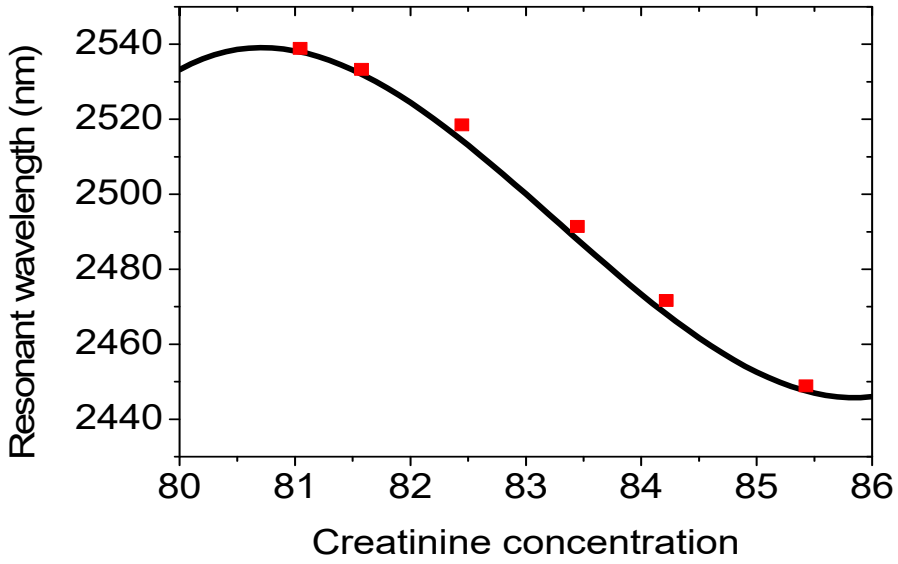

Figure 10. Resonant wavelength versus creatinine concentration for a ternary photonic crystal at $\theta_0 = 60^\circ$, $h_f = 5.5$ µm, and $N = 4$.

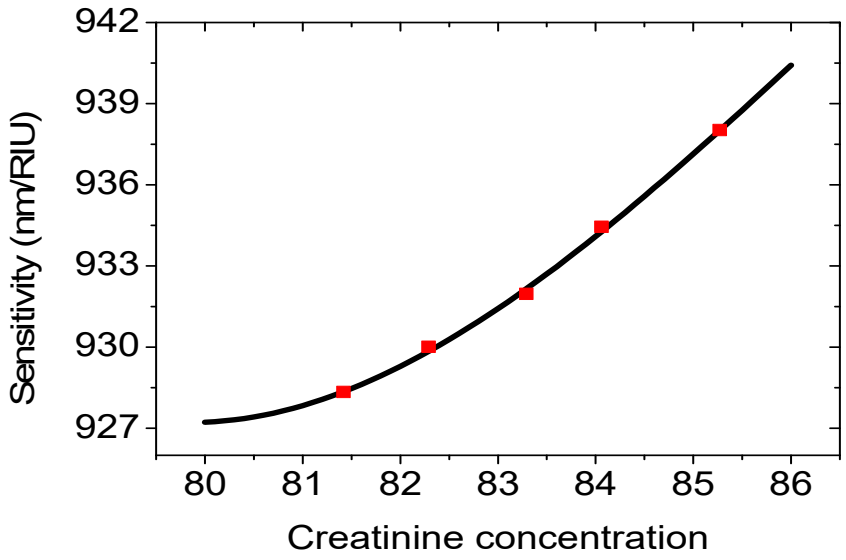

Figure 11. The sensitivity as a function of creatinine concentration for a proposed ternary photonic crystal at $\theta_0 = 60^\circ$, $h_f = 5.5$ µm, and $N = 4$.

Table 6. The present study's sensitivity in comparison to the most recent biosensors that have been published.

Techniques/Structures	Year	*S* (nm/RIU)	References
A PC made of nanocomposite materials as a biosensor	2019	43	[30]
Biosensor using array of split ring resonators	2019	657.5	[31]
1D-PC based biosensor for creatinine concentration detection	2020	306.25	[26]
1D-PC with extra layers on the sensing sample's sides	2021	161	[32]
Creatinine concentration biosensor using a 1D-defective photonic structure	2021	640.29	[27]
A layer of nano-composite based a 1D-PC	2022	893	[33]
Ternary PC based on titanium nitride sandwiched between Si and SiO_2	2022	938.02	Current work

4. Conclusions

1D defective TPC with the structure air/$(Si/TiN/SiO_2)^4$/cavity layer/$(Si/TiN/SiO_2)^4$/air was tested as a biophotonic sensor device for the creatinine concentration detection in a blood serum sample. We constructed the formulation of transfer matrix that was employed with the help of mathematical software to investigate these outcomes. At oblique incidence, TE polarization shows performance better than TM polarization. With any variation in the creatinine concentration, the proposed design demonstrates excellent tuning. It is also noted that the performance of the biosensor can be modified by related factors, such as angle of incidence and thickness of the cavity layer. Increasing the incident angle enhances the sensitivity of the suggested structure. It was observed that when the angle of incidence increases, the peak's intensity acceptably decreased until it reached an angle of $\theta_0 = 60^\circ$, at which point the intensity began to unsatisfactorily decline. Thus, the optimum angle was selected as $\theta_0 = 60^\circ$. In addition, the sensitivity of the proposed biosensor showed dramatic improvement with the growing of the cavity layer's thickness. We found the optimum thickness to be $h_f = 5.5$ µm. The maximum sensitivity of the proposed biophotonic sensor was found to be 938.02 nm/RIU. It is clear our proposed structure demonstrates high sensitivity for the detection of creatinine concentration. Moreover, our biosensor is economical, tunable, and has a simple architecture that gives it a good technique for the detection of creatinine concentration. The aforementioned findings could find an applicable and real path for any design related to biosensing.

Author Contributions: Conceptualization, M.G.D. and Y.T.; methodology and software, M.G.D., A.P. and A.H.G.; validation and discussion, M.G.D., K.M.A., L.K.S. and B.R.A.; writing and editing, M.G.D. and A.N.Z.R. All authors have read and agreed to the published version of the manuscript.

Funding: Deanship of Scientific Research—Research Center at King Khalid University in Saudi Arabia for funding this research (code number: RGP 2/23/43).

Data Availability Statement: Not applicable.

Acknowledgments: The authors are thankful to the Deanship of Scientific Research—Research Center at King Khalid University in Saudi Arabia for funding this research (code number: RGP 2/23/43).

Conflicts of Interest: The authors declare no conflict of interest.

References

1. Ahmed, A.M.; Elsayed, H.A.; Mehaney, A. High-Performance Temperature Sensor Based on One-dimensional Pyro electric Photonic Crystals Comprising Tamm/Fano Resonances. *Plasmonics* **2020**, *16*, 547–557. [CrossRef]
2. Aly, A.H.; Mohamed, D.; Zaky, Z.A.; Matar, Z.S.; El-Gawaad, N.S.A.; Shalaby, A.S.; Tayeboun, F.; Mohaseb, M. Novel Biosensor Detection of Tuberculosis Based on Photonic Band Gap Materials. *Mater. Res.* **2021**, *24*, e20200483. [CrossRef]
3. Daher, M.G.; Jaroszewicz, Z.; Zyoud, S.H.; Panda, A.; Abd-Elnaby, M.; Mahmoud, M.A.E.; Ahmed, N.Z.R. Design of A novel Detector Based on Photonic Crystal Nanostructure for Ultra-High Performance Detection of Cells with Diabetes. *Opt. Quantum Electron.* **2022**, *54*, 701. [CrossRef]
4. Almawgani, A.H.M.; Taya, S.A.; Daher, M.G.; Alhawari, A.R.H.; Colak, I.; Patel, S.K. Design of a Novel Protein Sensor of High Sensitivity Using a Defective Ternary Photonic Crystal Nanostructure. *Silicon* **2022**, 1–8. [CrossRef]
5. Wu, F.; Wu, J.; Fan, C.; Guo, Z.; Xue, C.; Jiang, H.; Sun, Y.; Li, Y.; Chen, H. Omnidirectional optical filtering based on two kinds of photonic band gaps with different angle-dependent properties. *Eur. Lett.* **2020**, *129*, 34004. [CrossRef]
6. Bikbaev, R.G.; Vetrov, S.Y.; Timofeev, I.V. Hyperbolic metamaterial for the Tamm plasmon polariton application. *J. Opt. Soc. Am. B* **2020**, *37*, 2215–2220. [CrossRef]
7. Boutami, S.; Benbakir, B.; Leclercq, J.; Viktorovitch, P. Compact and polarization controlled 1.55 µm vertical-cavity surface-emitting laser using single-layer photonic crystal mirror. *Appl. Phys. Lett.* **2007**, *91*, 071105. [CrossRef]
8. Almawgani, A.H.M.; Daher, M.G.; Taya, S.A.; Colak, I.; Patel, S.K.; Ramahi, O.M. Highly sensitive nano-biosensor based on a binary photonic crystal for cancer cell detection. *Opt. Quantum Electron.* **2022**, *54*, 554. [CrossRef]
9. Zhao, X.; Hua, L.; Jiang, G.; Cheng, J.; Xiong, Q. A novel polarization filter based on photonic crystal fiber with a single Au-coated air hole and semi-hourglass structure. *Plasmonics* **2019**, *14*, 1725–1733. [CrossRef]
10. Cui, L.; Du, G.; Ng, J. Angle-independent and -dependent optical binding of a one-dimensional photonic hypercrystal. *Phys. Rev. A* **2020**, *102*, 023502. [CrossRef]
11. Taya, S.A.; Daher, M.G. Properties of defect modes of one-dimensional quaternary defective photonic crystal nanostructure. *Int. J. Smart Grid-Ijsmartgrid* **2022**, *6*, 29–39.
12. Segovia-Chaves, F.; Vinck-Posada, H. Dependence of the defect mode with temperature, pressure and angle of incidence in a 1D semiconductor-superconductor photonic crystal. *Phys. C Supercond. Appl.* **2018**, *553*, 1–7. [CrossRef]
13. Summers, N.; Johnsen, G.; Mogstad, A.; Løvås, H.; Fragoso, G.; Berge, J. Underwater Hyperspectral Imaging of Arctic Macroalgal Habitats during the Polar Night Using a Novel Mini-ROV-UHI Portable System. *Remote Sens.* **2022**, *14*, 1325. [CrossRef]
14. Baker, J.E.; Sriram, R.; Miller, B.L. Two-dimensional photonic crystals for sensitive microscale chemical and biochemical sensing. *Lab. Chip.* **2015**, *21*, 971–990. [CrossRef]
15. Segovia-Chaves, F.; Vinck-Posada, H. Tuning of the defect mode in a 1D superconductor-semiconductor crystal with hydrostatic pressure dependent frequency of the transverse optical phonons. *Phys. C Supercond.* **2018**, *556*, 7–13. [CrossRef]
16. Chen, T.; Han, Z.; Liu, J.; Hong, Z. Terahertz gas sensing based on a simple one-dimensional photonic crystal cavity with high-quality factors. *Appl. Opt.* **2014**, *53*, 3454–3458. [CrossRef]
17. Aly, A.H.; Ghany, S.S.A.; Fadlallah, M.; Salman, F.; Kamal, B. Transmission and temperature sensing characteristics of a binary and ternary photonic band gap. *J. Nanoelectron. Optoelectron.* **2015**, *10*, 9–14. [CrossRef]
18. Ayyanar, N.; Raja, G.T.; Sharma, M.; Kumar, D.S. Photonic Crystal Fiber-Based Refractive Index Sensor for Early Detection of Cancer. *IEEE Sens. J.* **2018**, *18*, 7093–7099. [CrossRef]
19. Raveendran, J.; Resmi, P.E.; Ramachandran, T.; Nair, B.G.; Babu, T.G. Fabrication of a disposable non-enzymatic electrochemical creatinine sensor. *Sens. Actuators B* **2017**, *243*, 589–595. [CrossRef]
20. Zeng, C.; Luo, C.; Hao, L.; Xie, Y. The research on magnetic tunable characteristics of photonic crystal defect localized modes with a defect layer of nanoparticle. *Chin. Opt. Lett.* **2014**, *12*, 11602. [CrossRef]
21. Junge, W.; Wilke, B.; Halabi, A.; Klein, G. Determination of reference intervals for serum creatinine, creatinine excretion and creatinine clearance with an enzymatic and a modified Jaff´e method. *Clin. Chim. Acta* **2004**, *344*, 137–148. [CrossRef] [PubMed]
22. Yao, T.; Kotegawa, K. Simultaneous flow-injection assay of creatinine and creatinine in serum by the combined use of a 16-way switching valve, some specific enzyme reactors and a highly selective hydrogen peroxide electrode. *Anal. Chim. Acta* **2002**, *462*, 283–291. [CrossRef]
23. Sharma, A.C.; Jana, T.; Kesavamoorthy, R.; Shi, L.; Virji, M.A.; Finegold, D.N.; Asher, S.A. A general photonic crystal sensing motif: Creatinine in bodily fluids. *J. Am. Chem. Soc.* **2004**, *126*, 2973. [CrossRef] [PubMed]
24. Panda, A.; Daher, M.G.; Pukhrambam, P.D.; Wu, F. Study of titanium nitride (TiN) as a novel plasmonic material for realization of Tamm-plasmon-polariton-based blood plasma sensor. *Opt. Quantum Electron.* **2022**, *54*, 796. [CrossRef]
25. Daher, M.G.; Taya, S.A.; Colak, I.; Vigneswaran, D.; Olaimat, M.M.; Patel, S.K.; Ramahi, O.M.; Almawgani, A.H. Design of a nano-sensor for cancer cell detection based on a ternary photonic crystal with high sensitivity and low detection limit. *Chin. J. Phys.* **2022**, *77*, 1168–1181. [CrossRef]
26. Aly, A.H.; Mohamed, D.; Mohaseb, M.A.; El-Gawaad, N.S.A.; Trabelsi, Y. Biophotonic sensor for the detection of creatinine concentration in blood serum based on 1D photonic crystal. *RSC Adv.* **2020**, *10*, 31765–31772. [CrossRef]
27. Gandhi, S.; Awasthi, S.K.; Aly, A.H. Biophotonic sensor design using a 1D defective annular photonic crystal for the detection of creatinine concentration in blood serum. *RSC Adv.* **2021**, *11*, 26655–26665. [CrossRef]

28. Taya, S.A.; Daher, M.G.; Colak, I.; Ramahi, O.M. Highly sensitive nano-sensor based on a binary photonic crystal for the detection of mycobacterium tuberculosis bacteria. *J. Mater. Sci. Mater. Electron.* **2021**, *32*, 28406–28416. [CrossRef]
29. Daher, M.G.; Taya, S.A.; Colak, I.; Ramahi, O.M. Design of a novel optical sensor for the detection of waterborne bacteria based on a photonic crystal with an ultra-high sensitivity. *Opt. Quantum Electron.* **2022**, *54*, 108. [CrossRef]
30. Ramanujam, N.R.; Amiri, I.; Taya, S.A.; Olyaee, S.; Udaiyakumar, R.; Pandian, A.P.; Wilson, K.S.J.; Mahalakshmi, P.; Yupapin, P.P. Enhanced sensitivity of cancer cell using one dimensional nano composite material coated photonic crystal. *Microsyst. Technol.* **2019**, *25*, 189–196. [CrossRef]
31. Nejad, H.E.; Mir, A.; Farmani, A. Supersensitive and Tunable Nano-Biosensor for Cancer Detection. *IEEE Sensors J.* **2019**, *19*, 4874–4881. [CrossRef]
32. Bijalwan, A.; Singh, B.K.; Rastogi, V. Analysis of one-dimensional photonic crystal-based sensor for detection of blood plasma and cancer cells. *Opt. Int. J. Light Electron Opt.* **2021**, *226*, 165994. [CrossRef]
33. Almawgani, A.H.M.; Suthar, B.; Bhargava, A.; Taya, S.A.; Daher, M.G.; Wu, F.; Colak, I. Sucrose concentration detector based on a binary photonic crystal with a defect layer and two nanocom-posite layers. *Z. Für Nat. A—Sect. A J. Phys. Sci.* **2022**, *77*, 909–919.